J6.5 RECENT CLIMATE VARIABILITY IN ANTARCTICA FROM SATELLITE-DERIVED TEMPERATURE DATA

David P. Schneider* and Eric J. Steig
University of Washington, Seattle, WA
Josefino Comiso
NASA Goddard, Greenbelt, MD

1. INTRODUCTION

Considerable interest has been shown in documenting and explaining recent climate changes in the Antarctic (e.g. Vaughan et al. 2001, Thompson and Solomon, 2002). Because Antarctic meteorological observations are short and sparsely distributed, questions remain about both the sign and magnitude of trends across most of the continent. Furthermore, relatively little is known about Antarctica's background climate variability. Such knowledge is needed both to place recent climate trends into context and to understand what is recorded in "proxy" ice core records from the continent.

Satellite-derived temperature data present an opportunity to examine Antarctica's climate variations in areas which are not represented by stations or reliably depicted in atmospheric analysis and reanalysis data. Furthermore, principal modes of temperature variability obtained from the satellite data provide a means by which to empirically reconstruct temperature variations prior to the satellite era. Reconstructed temperature records in turn provide a template against which ice core records can be calibrated, offering the potential to reconstruct Antarctic climate even further in the past. This is an important goal, since in even the most recent comprehensive global scale climate reconstructions [e.g. Mann and Jones 2003], the Antarctic region remains a large unknown due to lack of available data.

2. APPROACH

We summarize the study of Schneider et al. (2004) which compares empirical modes of variability determined from passive microwave brightness temperature (T_B) and temperature retrievals from thermal infrared (T_{IR}) satellite observations over the Antarctic continent. The longer-wavelength microwave data (from the 37 GHz vertical polarization channel) have the advantage of being largely unaffected by clouds, yet they are affected by the thermal and scattering properties of the upper ~1m of snow and firn. The T_{IR} data more directly measure surface temperature, yet they must be carefully screened for the presence of clouds. Through Maximum Covariance Analysis (MCA) (von Storch and Zweirs 1999), the two data sets are shown to have a strong covariance, largely representing surface temperature variability. Variability in the passive microwave data is specifically documented by Schneider and Steig (2002), while the physical mechanisms which relate this variability to surface temperature are discussed by Winebrenner et al. (2004).

We examine the relationship between surface temperature variability and atmospheric circulation through comparison of the empirical modes of the satellite data sets with NCEP-NCAR reanalysis geopotential height anomalies at the 500-hPa level. We show that, overall, the Southern Annular Mode (SAM) explains the greatest variance in Antarctic temperatures. Some previous studies have reasoned that ENSO explains the greatest share of the remaining variance (e.g Kwok and Comiso 2002). However, we show that the second most important influence is not simply described by ENSO directly, but rather, reflects a combination of patterns previously referred to as the Pacific South American and wavenumber-3 patterns. We also suggest that blocking may be responsible for driving strong temperature trends in a little-studied region (0°-90°E) of East Antarctica. Finally, through calibrations of station data, we make a preliminary reconstruction of Antarctic temperatures back to 1960.

3. RESULTS

3.1 Major modes in the satellite data

The leading modes of monthly satellite-derived temperature anomalies from 1982-1999, which explain the most covariance between the two data

**Corresponding author address*: David P. Schneider, University of Washington, Department of Earth and Space Sciences, Campus Box 351310, Seattle, WA 98103. email: schneidd@u.washington.edu

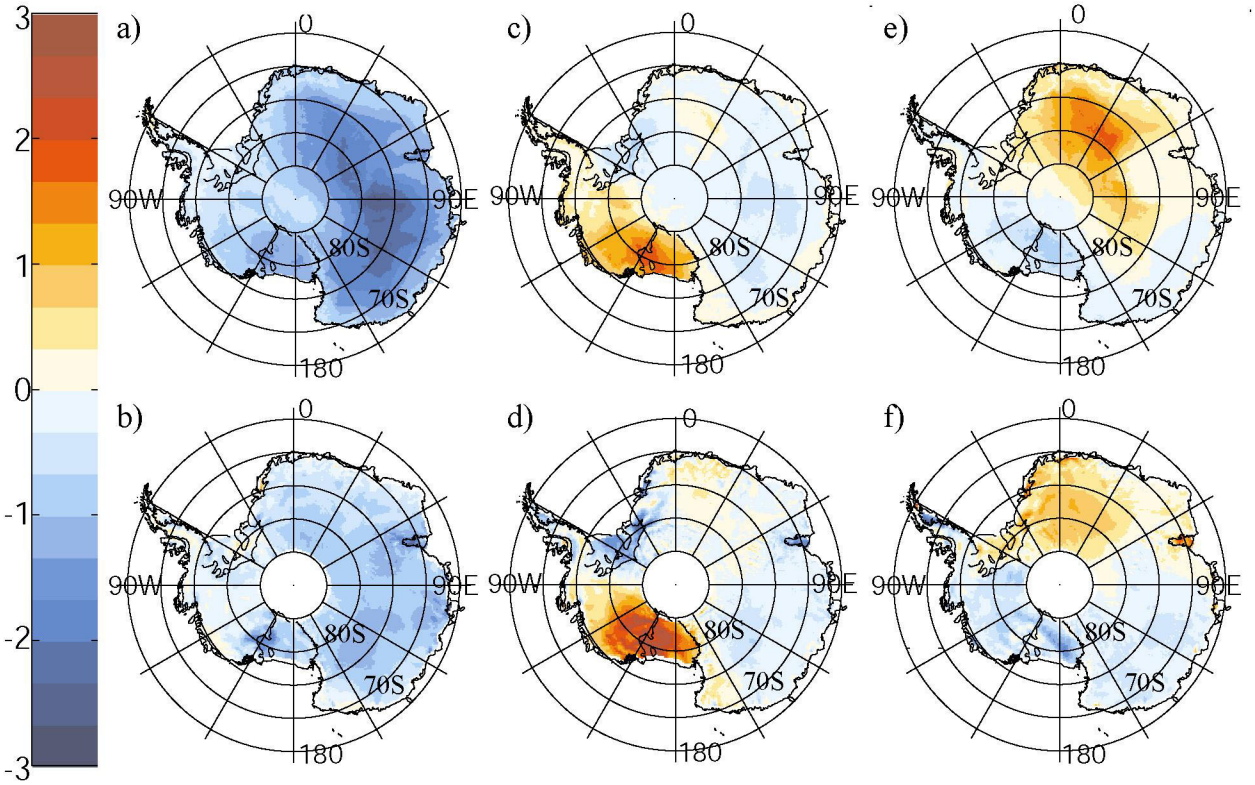

Figure 1. Heterogeneous regression maps from MCA of T_{IR} and T_B fields. The top panels (a,c,e) are covariances from the T_{IR} field regressed upon the first, second, and third normalized T_B expansion coefficients, respectively. The bottom panels (b,d,f) are covariances from the T_B field regressed upon the first, second, and third normalized T_{IR} expansion coefficients, respectively. Color is in units of K, corresponding to one standard deviation of the respective expansion coefficient.

sets, are shown in Figure 1. The first four maps are quite similar to those obtained when standard EOF analysis is applied to each data set independently, implying that the two data sets are strongly related. Specifically, these are heterogeneous regression maps derived from MCA applied to the data and are similar to cross-regressions, corresponding to the anomaly in the field on the map associated with one standard deviation of the opposite field's expansion coefficient time series (expansion coefficient for mode 1 T_{IR} is denoted as T_{IR}x-1, for mode 2, T_{IR}x-2, and so on).

For mode 1, the T_{IR} field regressed onto T_Bx1 (Fig. 1a) is similar to the first EOF of T_{IR} anomalies, although less variance in T_{IR} is explained (23%). The T_B field regressed onto T_{IR}x1 (Fig. 1b) produces a pattern that is more smoothly varying than the first EOF of T_B (see Schneider and Steig 2002, Fig. 2a), and explains 11% of the variance. The amplitudes in Fig. 1b are smaller than those in Fig. 1a, implying attenuation of the surface temperature signal. This mode shows the same sign of temperature anomalies across much of Antarctica, with the exception of the northern Antarctic Peninsula, and has the strongest variance in the high plateau of East Antarctica.

In Fig. 1c, the T_{IR} field is regressed onto T_Bx2, explaining 3% of the variance in T_{IR}, and the resulting pattern is similar to the second EOF of T_{IR}. Likewise, regression of the T_B field onto T_{IR}x2 (Fig. 1d), explains 4% of the variance, and produces a heterogeneous map similar to the second EOF of T_B. In this pair of maps, the amplitudes are comparable in magnitude, consistent with little attenuation, a shallow penetration depth, and low microwave emissivity in the Ross Sea sector of Antarctica. In this mode, the largest temperature anomalies occur in the vicinity of 150°W over the Ross Ice Shelf and the Siple Coast. The anomalies taper off dramatically and change sign towards East Antarctica.

A third mode is diagnosed with MCA that was not prominent in the EOF results for the data sets when considered separately (although this third MCA mode correlates well with the fourth mode in T_{IR} data alone and the fifth mode in T_B data alone). It is retained for discussion because it projects onto the linear trends in the T_{IR} and T_B data sets

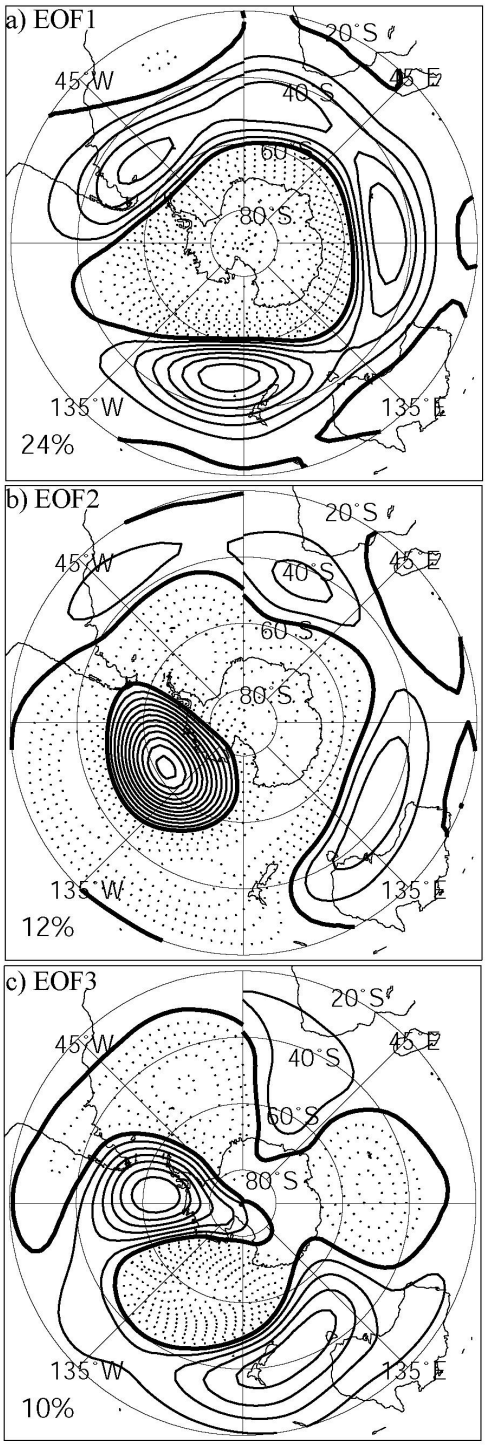

Figure. 2. The leading modes in monthly 500-hPa geopotential height, 1982-1999. The (a) first, (b) second, and (c) third EOFs, shown as the Z500 data regressed upon the leading normalized PCs. Percentage of variance explained indicated at lower left. Contour interval 5m, zero contour heavy solid line, negative contours dotted, positive contours solid.

and is reproducible. Because the T_{IR}x3 and T_Bx3 expansion coefficient time series have upward trends (not shown), these time series and the T_{IR} and T_B gridpoint data are both detrended prior to the construction of the heterogeneous regression maps in order to avoid spurious correlations. If the trends are retained in the time series, the heterogeneous maps of mode 3 look very similar to annual mean trends in the T_{IR} and T_B data sets (see Kwok and Comiso 2002, Fig. 2, for trends in T_{IR}). Therefore, care must be taken not to include spurious correlations of unrelated trends in the maps. The map with T_{IR} data regressed onto T_Bx3 explains 4% of T_{IR} variance and shows positive anomalies in T_{IR} throughout much of East Antarctica (Fig. 1e). The anomalies of greatest magnitude occur from 0° to 60°E. Similarly, the map of T_B data regressed onto T_{IR}x3 explains 4% of T_B variance and shows positive T_B anomalies, but of weaker magnitude, in the same area of East Antarctica (Fig. 1f).

3.2 Major modes in atmospheric circulation

To define the leading patterns of SH atmospheric circulation during the time period of this study, EOF analysis is applied to monthly Z500 anomaly data poleward of 20°S. For equal-area weighting, the data are weighted by the square root of the cosine of their latitude. The original unweighted Z500 data are regressed against each normalized PC, showing anomalies corresponding to one standard deviation of the corresponding PC. Three patterns of interest are resolved, explaining 24%, 12%, and 10% of the (weighted) variance respectively. The second and third patterns are not well separated under the criteria of North et al. (1982). However, they have been reported by a number of studies and found in many different data sets (e.g. Cai and Watterson 2002; Mo and White 1985). Our results are consistent with the definition of the first Z500 pattern as the SAM (Fig. 2a), the second Z500 pattern as the Pacific South American (PSA) pattern (Fig.2b), and the third pattern as the zonal wavenumber-3 pattern (Fig. 2c) as named by other studies (Cai and Watterson 2002; Mo 2000). The third pattern is sometimes called the PSA-2 pattern (Mo 2000). The signs are displayed for consistency with the modes in T_{IR} and T_B and the regression patterns discussed below.

3.3 Covariance of temperature and circulation anomalies

Regressions of T_{IR} data onto the normalized PCs of the three leading Z500 patterns are shown

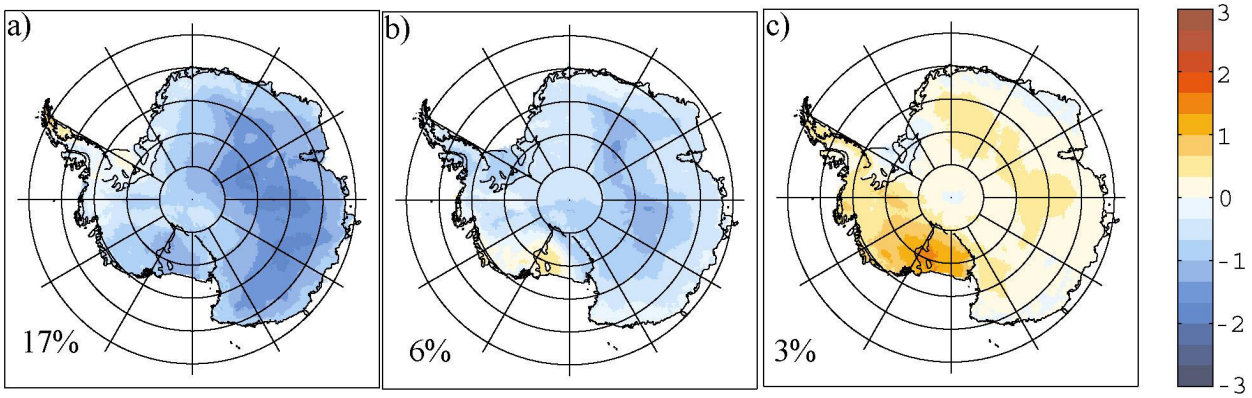

Figure 3. Regressions of T_{IR} gridpoint data upon the first three Z500 normalized PCs (a-c, respectively). Percentage of variance explained indicated in lower left. Color scale is in K, corresponding to one standard deviation of the respective PC time series.

in Fig. 3. The SAM explains 17% of the variance in T_{IR} anomalies (Fig. 3a), the PSA pattern explains 6% of the variance (Fig. 3b), and the zonal wavenumber-3 pattern explains 3% of the variance (Fig. 3c). The first regression pattern is quite similar to the first T_{IR} EOF or heterogeneous regression map. During the positive phase of the SAM, relatively strong westerlies encircle Antarctica near 60°S, which tends to enhance warm air advection over the northern Peninsula, while the cool anomalies on the rest of the continent are indicative of adiabatic cooling (Thompson and Wallace 2000).

As seen in Fig. 3b, in East Antarctica, the PSA pattern explains much less variance in surface temperature than does the SAM, but the spatial structures of temperature anomalies are generally similar. In the Peninsula and most of West Antarctica, the PSA pattern explains variability of the same sign as in East Antarctica. However, the PSA pattern is associated with temperature anomalies of opposite sign near 150°W, 75°S, consistent with the anticyclonic 500-hPa height anomaly centered near 60°S, 125°W (Fig. 2b).

As shown in Fig. 3c., the wavenumber-3 pattern explains positive temperature anomalies over the same area of West Antarctica associated with the second surface temperature mode, consistent with the strong positive and negative height anomalies centered along 60°S near 90°W and 155°W, respectively. The wavenumber-3 pattern also explains weak temperature anomalies of the same sign in East Antarctica, unlike the second temperature mode, in which West and East Antarctica are out of phase. This is likely due to the additional influence of the PSA pattern on the second surface temperature mode. While the PSA pattern in Z500 is associated with geopotential height fluctuations over East Antarctica, the wavenumber-3 pattern has very little correlation with height anomalies over this region.

As a consistency check, Z500 data are now regressed upon T_{IR} expansion coefficients from the leading MCA modes. As above, the time series of mode 3 are detrended prior to regression. Although T_{IR} expansion coefficients are used here for illustration, regressions involving T_B expansion coefficients are very similar. The first Z500 regression pattern (Fig. 4a) closely resembles the SAM pattern in Z500 (Fig. 2a), especially in the Eastern Hemisphere. In the west, the PSA (Fig. 2b) pattern appears to have an influence on both the first and second regression patterns (Fig. 4a and 4b). However, the second regression pattern (Fig. 4b) most strongly correlates with the Z500 wavenumber-3 pattern (Fig. 2c). The third regression pattern (Fig. 2c) resembles the SAM, but has anomalies of much weaker magnitude. The positive anomalies in East Antarctica near 45°E are suggestive of a ridge in the mid-troposphere extending inland through East Antarctica. This resembles the wintertime blocking episodes discussed by Hirasawa et al. (2000) and Enomoto et al. (1998), who documented warm, moist air being pumped from the north all the way to the polar plateau. The positive temperature anomalies associated with the third mode (Fig. 1e) correspond to the "strip" of annual mean warming on the East Antarctic ridge observed by Kwok and Comiso (2002). Inspection of monthly trends shows that in winter months, warming trends in T_{IR} occur over a much broader area than this strip, and Comiso (2000) described several anomalously warm July episodes in East Antarctica. Since the winter months account for most of the trend in the mode 3 expansion coefficients, it is likely that the events explained by mode 3 and these warm episodes are part of the same phenomenon.

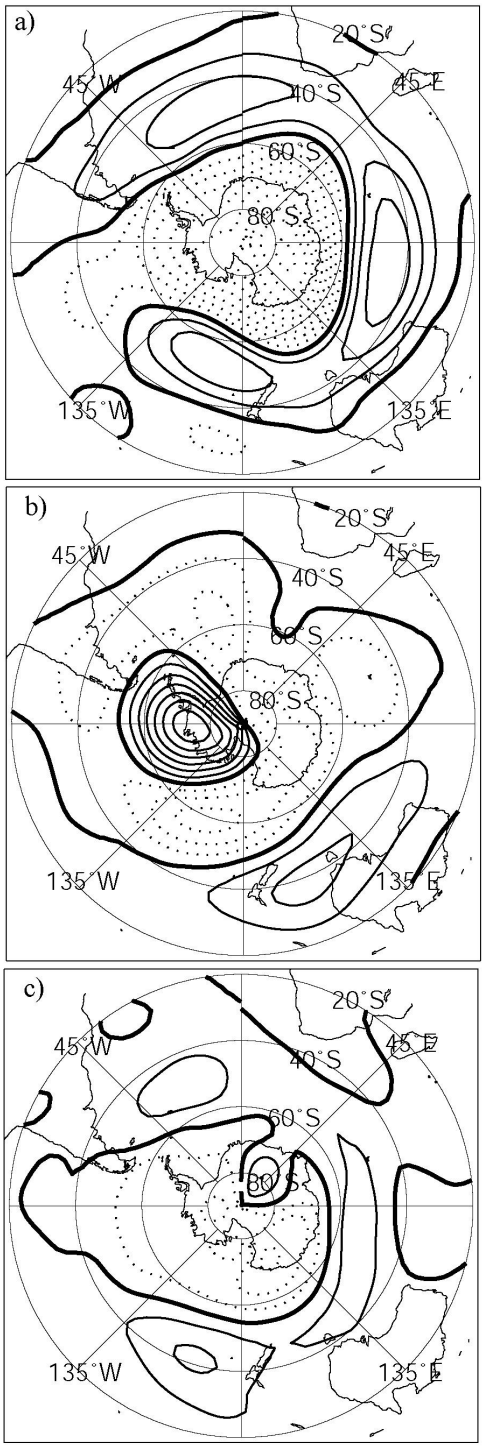

Figure. 4. Regression of Z500 data upon the (a) first, (b) second, and (c) third normalized T_{IR} expansion coefficients shown in Fig. 4. Units, contours as in Fig. 2.

3.4 Reconstruction of pre-satellite temperature variations

The satellite temperature data provide a basis on which to reconstruct Antarctic temperature variability, using the modes discussed above as calibration data for the longer weather station records. In this context, establishment of a clear relationship between Antarctic surface temperature variability and patterns of variability in extratropical SH atmospheric circulation is important because it increases confidence that empirical calibrations will have a physical justification. We primarily follow the EOF-based methods and assumptions of Mann et al. (1998), although over a more limited spatial domain.

Some preliminary results are shown in Fig. 5., including the correlation during the calibration interval (1982-1999) of a five mode EOF-based reconstructed data set and the original T_{IR} data on a monthly timescale. The mean variance explained on the continent during the calibration interval is 29%, 35%, and 36% for two-mode, four-mode, and five-mode based reconstructions, respectively. Stations are marked with an 'X', with the correlation between the station temperature time series from 1961-2002 and the reconstructed temperature at the nearest grid point indicated. A reconstruction with two modes explains 38% of the variance in station data, with four modes the variance explained improves to 50%, and with five modes, the variance explained is 54%. The small improvement with inclusion of the fifth mode represents the contribution of Faraday station, which is not significantly correlated with any of the other modes. There is a trade-off between explaining more variance by including more modes and placing constraints on the reconstruction of the first two, and best-understood modes. The first reconstructed principal component, which caries the signature of the SAM, is correlated with the original first principal component at r = .69 using a five mode template (r = .73 with a two-mode template), and is correlated at r = .72 with the 1968-1998 radiosonde-based SAM index of Thompson and Solomon (2002), as shown in Fig. 6.

4. DISCUSSION

Spatial and temporal patterns of T_{IR} and T_B variability, and more importantly, surface temperature variability, in Antarctica are consistent with the leading patterns of variability in extratropical SH atmospheric circulation. It is clear that the most important influence on Antarctic

temperature anomalies from month-to-month to interannual timescales is the SAM. This first mode is well separated from other modes in both Z500 data and the satellite data sets. On the basis of the original T_{IR} monthly data, strong temperature trends associated with this mode are not observed. However, inspection of trends by month over the length of the record shows that T_{IR} observations are consistent with a late spring and summer cooling trend, possibly driven by an increasing tendency of the SAM to stay in its positive phase during the late spring (Thompson and Solomon 2002). It is interesting to note, however, the leading reconstructed temperature PC, which explains most of the variance in the mean, shows an upward trend from 1961-2002. This is in contrast to the upward trend in the SAM, which would be expected to produce cooler temperatures. A comprehensive study of trends in Antarctic temperatures that are associated with this mode, and possibly the third mode as discussed below, requires further work.

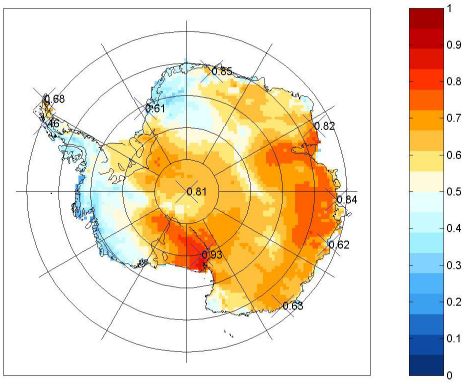

Figure 5. Reconstruction calibration statistics. Colors indicate the correlation (r) between original T_{IR} anomaly data and the reconstructed field during the calibration period. Station locations, 'X', with the correlation of the 1961-2002 station temperature anomaly timeseries and the nearest reconstructed T_{IR} grid point.

The PSA pattern has an influence on the first two surface temperature modes. The wavenumber-3 pattern of variability, however, has a relatively stronger influence on the second surface temperature mode, shown by its association with large temperature anomalies in the West Antarctic sector inland of the Ross and Amundsen seas. Anomalies of opposite sign in East Antarctica suggest that the PSA pattern exerts a stronger influence there. Since ENSO-related variability projects primarily onto the PSA and the wavenumber-3 patterns (Venegas 2003; Cai and Watterson 2002), Antarctic climate records can show ENSO-like spectra (e.g. Schneider and Steig 2002; Ichiyanagi et al. 2002; Bromwich and Rogers 2001). However, we find that the direct correlation of Antarctic temperatures with an ENSO index such as the SOI does not account for much temperature variance (variance explained is 0.5%, see Kwok and Comiso 2002; Schneider and Steig 2004).

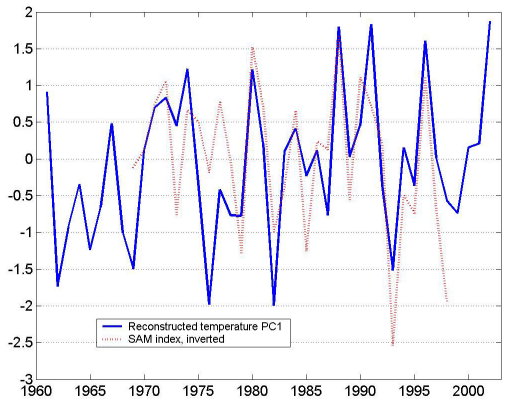

Figure 6. Smoothed versions (annual mean) of reconstructed temperature PC1 (solid blue line) and the inverted SAM index (dotted red line). Note that while the correlation between the two series is positive, the trends diverge.

Some persistent trends in the available satellite record are associated with the third mode, which cannot, within the scope of this study, be clearly linked to the principal patterns of atmospheric circulation variability. However, blocking events over inland East Antarctica have been documented with station data (Hirasawa et al. 2000; Enomoto et al. 1998) and provide a plausible explanation for the trends in temperature and the pattern seen in Z500 on our regression map (Fig. 4c). During these episodes, rises of ~40 K can occur in two days or less at remote interior stations such as Dome Fuji and Plateau, and T_a can take more than a month to return to its value before the rise (Enomoto et al. 1998; Kuhn et al. 1973). The upward trend in the T_{IR} and T_B expansion coefficients comes primarily from the winter months, when the blocking episodes most often occur and the surface temperature is extremely sensitive to circulation changes. In addition, changes in cloud cover and winds associated with blocking will destroy the surface inversion, adding to the magnitude of the surface temperature anomalies (Hirasawa et al. 2000). At present, however, the satellite record is too short to establish the long-term significance of the trends, and the monthly temporal resolution of this

study limits our ability to further characterize the causes of variability in the third temperature mode.

Currently, a gap exists between our understanding of Antarctica's short instrumental and satellite records, and deep ice cores from Antarctica (e.g. Petit et al., 1999; Morgan et al. 2002). Future work will include evaluating the stability of the temperature and circulation modes discussed here on longer timescales. Some prior work suggests that these modes have operated on a wide range of timescales. For instance, long ice core paleoclimate records from locations spread thousands of kilometers apart in East Antarctica are well correlated with each other on millennial timescales, while records from West Antarctica and some East Antarctic cores appear to reflect climate variations over a smaller region (Watanabe et al. 2003; Steig et al. 2000). A simple explanation of this is that East Antarctic isotopic records from the ice cores may be tied to the SAM over a large area (Noone and Simmonds 2002), while West Antarctic ice core records are more strongly linked to circulation variability in the Southern Pacific, which in turn is teleconnected to the tropical Pacific during strong El Niño and La Niña events (Bromwich et al. 2003). Century-scale reconstructions of the major modes of SH atmospheric circulation from tree rings (Jones and Widmann 2003) and a network of intermediate-depth Antarctic ice cores (Mayewski 2003) will help to fill in the gap between our understanding of modern climate variability and our theories of past climate variations.

5. REFERENCES

Bromwich, D. H. and A. N. Rogers, 2001: The El Niño-Southern Oscillation modulation of West Antarctic precipitation. *Ant. Res. Ser.,* **77**, 91-104.

Bromwich, D.H., A.J. Monaghan, and Z. Guo, 2003: Modeling the ENSO modulation of Antarctic climate in the late 1990s with Polar MM5, *J. Climate*, in press.

Cai, W., and I.G. Watterson, 2002: Modes of interannual variability of the southern hemisphere circulation simulated by the CSIRO climate model. *J. Climate,* **15**, 1159-1174.

Comiso, J. C., 2000: Variability and trends in Antarctic surface temperatures from in situ and satellite infrared measurements, *J. Climate*, **13**, 1674-1696.

Enomoto, H., and Coauthors, 1998: Winter warming over Dome Fuji, East Antarctica, and the semiannual oscillation in the atmospheric circulation, *J. Geophys. Res.,* **103**, D18, 23,103-23,111.

Hirasawa, N., H. Nakamura, and T. Yamanouchi, 2000: Abrupt changes in meteorological conditions observed at an inland Antarctic station in association with wintertime blocking, *Geophys. Res. Lett.,* **27** (13), 1911-1914.

Ichiyanagi, K., Numaguti, A., and K. Kata, 2002: Interannual variation in stable isotopes in Antarctic precipitation in response to El Niño -Southern Oscillation, *Geophys. Res. Lett.,* **29**(1), 10.129/2000GL012815.

Jones, J., and M. Widmann, 2003: Instrument and tree ring based estimates of the Antarctic Oscillation, *J. Climate*, **16**(21), 3511-3524.

Kwok, R., and J.C. Comiso, 2002: Spatial patterns of variability in Antarctic surface temperature: Connections to the Southern Hemisphere Annular Mode and the Southern Oscillation, *Geophys. Res. Lett.,* **29**(14), 10.1029/2002GL015415.

Mann, M.E., R.S. Bradley, and M.K. Hughes, 1998: Global-scale temperature patterns and climate forcing over the past six centuries, *Nature*, **392**, 779-787.

Mann. M.E., and P.D. Jones, 2003: Global surface temperatures over the past two millenia, *Geophys. Res. Lett*., **30**(15), doi:10.129/2003GL017814.

Mayewski, P.A., 2003: Antarctic Oversnow Traverse-based Southern Hemisphere Climate Reconstruction *EOS, Transactions, American Geophysical Union*, **84**(12), 205.

Mo, K.C., and R.W. Higgins, 1998: The Pacific South American modes and tropical convection during the Southern Hemisphere winter, *Mon. Weather. Rev*., **126**, 1581-1596.

Mo, K.C., 2000: Relationships between low-frequency variability in the Southern Hemisphere and sea surface temperature anomalies, *J. Climate*, **13**, 3599-3610.

Morgan, V., M. Delmotte, T. van Ommen, J. Jouzel, J. Chappellaz, S. Woon, V. Masson-Delmotte, and D. Raynaud, 2002: Relative timing of deglacial and climate events in Antarctica and Greenland, *Science*, **297**, 1862-1864.

Noone, D., and I. Simmonds, 2002: Annular variation in moisture transport mechanisms and the abundance of $\delta^{18}O$ in Antarctic Snow, *J. Geophys. Res*., **107**(D24), 4742, 10.129/2002JD00262.

Petit, J.R., and Coauthors, 1999: Climate and atmospheric history of the past 420,000 years from the Vostok ice core, Antarctica, *Nature*, **399**, 429-436.

Schneider, D.P., and E.J. Steig, 2002: Spatial and temporal variability of Antarctic ice sheet microwave brightness temperatures, *Geophys. Res. Lett*., **29**(20), doi:10.129/2002GL15490.

Schneider, D.P., E.J. Steig, and J.C. Comiso, 2004: Recent Climate Variability in Antarctica from Satellite-derived temperature data, *J. Climate*, in press.

Steig, E.J., Morse, D.L., Waddington, E.D., Stuiver, M., Grootes, P.M., Mayewski, P.A., Whitlow, S.L. and M.S. Twickler, 2000: Wisconsinan and Holocene climate history from an ice core at Taylor Dome, western Ross Embayment, Antarctica. *Geograf. Annal.* **82A**, 213-235.

Thompson, D.W J. and J.M. Wallace, 2000: Annular Modes in the extratropical circulation. Part I: Month-to-month variability, *J. Climate*, **13**, 1000-1016.

Thompson, D.W.J., and S. Solomon, 2002: Interpretation of recent southern hemisphere climate change, S*cience,* **296**, 895-899.

Vaughan, D.G., G.J. Marshall, W.M. Connolley, J.C. King, and R. Mulvaney, 2001: Devil in the detail, *Science*, 293, 1777-1779.

Venegas, S.A., 2003: The Antarctic Circumpolar Wave: A combination of two signals?, *J. Climate*, 16(15), 2509-2525.

von Storch, H., and F.W. Zweirs, 1999: *Statistical Analysis in Climate Research*. Cambridge University Press, 484 pp.

Watanabe, O., J. Jouzel, S. Johnsen, F. Parrenin, H. Shoji, and N. Yoshida, 2003: Homogeneous climate variability across East Antarctica over the past few glacial cycles, *Nature*, **422**, 509-512.

Winebrenner, D.P., E.J. Steig, and D.P. Schneider, 2004, Temporal covariation of Surface and microwave brightness temperatures in Antarctica, with implications for the observation of surface temperature variability in Antarctica using satellite data, *Ann. Glaciol*, in press.